Received: 6 October 2023 | Revised: 22 November 2023 | Accepted: 10 December 2023

DOI: 10.1002/agt2.483

Aggregate WILEY

RESEARCH ARTICLE

The dynamics of PEG-coated nanoparticles in concentrated protein solutions up to the molecular crowding range

Ferdinand Otto[1] | **Francesco Dallari**[2] | **Fabian Westermeier**[3] | **D. C. Florian Wieland**[4] | **Wolfgang J. Parak**[1,5] | **Felix Lehmkühler**[3,5] | **Florian Schulz**[1]

[1]Center for Hybrid Nanostructures, Universität Hamburg, Hamburg, Germany

[2]Department of Physics and Astronomy "Galileo Galilei", University of Padova, Padova, Italy

[3]Deutsches Elektronen-Synchrotron DESY, Hamburg, Germany

[4]Institute of Metallic Biomaterials, Helmholtz-Zentrum Hereon, Geesthacht, Germany

[5]The Hamburg Centre for Ultrafast Imaging, Hamburg, Germany

Correspondence
Felix Lehmkühler, Deutsches Elektronen-Synchrotron DESY, Notkestr. 85, 22607 Hamburg, Germany.
Email: felix.lehmkuehler@desy.de

Florian Schulz, Center for Hybrid Nanostructures, Universität Hamburg, Luruper Chaussee 149, 22761 Hamburg, Germany.
Email: florian.schulz@physik.uni-hamburg.de

Funding information
Deutsche Forschungsgemeinschaft, Grant/Award Numbers: GRK 2536, EXC 2056; European Synchrotron Radiation Facility, Grant/Award Number: SC 5173

Abstract

Polymer-coated nanoparticles are widely studied in the context of nanomedicine and it is therefore of utmost importance to understand not only how their structure but also how their colloidal dynamics are affected by physiologically relevant conditions. A characteristic feature of the cytosol of cells is the very high concentration of proteins among other matrix components, often termed macromolecular crowding. Here, the structure and colloidal dynamics of poly(ethylene glycol) (PEG)-coated gold nanoparticles in the presence of bovine serum albumin (BSA) concentrations ranging from 0 to 265 mg/mL are studied with X-ray photon correlation spectroscopy. For protein–nanoparticle mixtures with high BSA concentrations, comparable to intracellular levels, a significant deviation of the apparent viscosity from expectations for pure BSA solutions is found. The findings strongly indicate that the nanoscopic viscous properties of the dense protein solutions are significantly affected by the nanoparticles. At these high concentrations, the colloidal stability of the samples depends on the molecular weight of the coating PEG–ligand, whereas at lower concentrations no differences are observed.

KEYWORDS

aggregation, nanoparticles, PEG, polymers, proteins, XPCS

1 | INTRODUCTION

One major field envisioned for nanoparticle (NP)-based applications is medicine and in this context the behavior of NPs in biological media is the subject of intense research efforts.[1–7]

When NPs are introduced into the body, they encounter various physiological environments with different physicochemical conditions, including pH, ionic strength, and local molecular composition, but also viscosity. Of particular significance is crowded and protein-rich fluids, such as blood, interstitial fluids, and intracellular fluids, which are present in the cytosol (though NPs most of the time will not be free in the cytosol but rather are trapped in endosomal vesicles) (Figure 1A).[8–10] The protein concentration in the cytosol can reach values of up to 400 mg/mL, and for this condition, the term macromolecular crowding has been established.[8,11–16] The relevance of macromolecular crowding for dynamics and binding properties in cells has received increasing attention within the last two decades. Macromolecular crowding affects the diffusive properties, stability, and folding of proteins. While many attempts to understand the impact of crowding have been of theoretical nature due to the cellular complexity,[17,18] among the experimental studies, fluorescence correlation spectroscopy (FCS),[19–21] nuclear magnetic resonance spectroscopy,[22–26] and neutron scattering[27] have been used to study protein dynamics and protein–protein interactions in crowded environments. In particular, in situ FCS and single-particle tracking studies in living cells revealed anomalous and spatially heterogeneous dynamics with indications of different subdiffusive mechanisms.[20,28,29] More recently, X-ray photon correlation spectroscopy (XPCS) has emerged as a powerful technique to study complex dynamics of soft matter

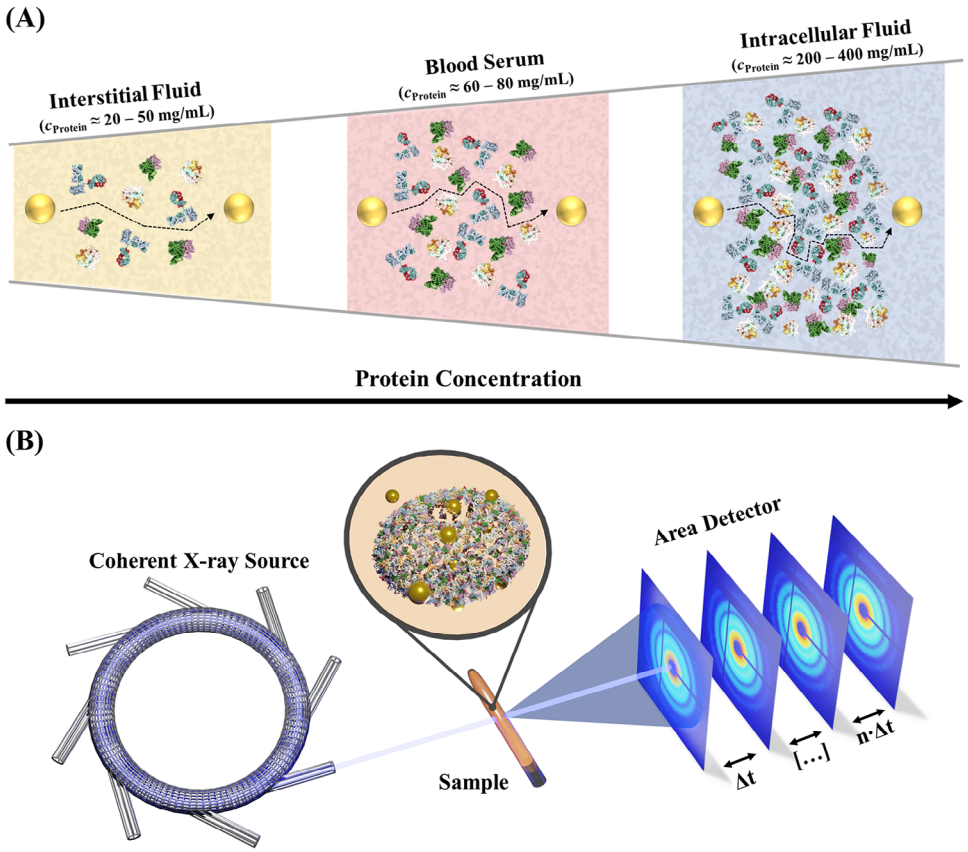

FIGURE 1 (A) Schematic representation of protein concentrations in different physiological fluids. (B) Scheme of the X-ray photon correlation spectroscopy setup.

systems.[30] In XPCS experiments, (partially) coherent X-rays generated by a synchrotron radiation source create fluctuating speckle patterns on an area detector upon interacting with a dynamic sample, which are then correlated over time. A schematic of an XPCS measurement is visualized in Figure 1B. Recently, XPCS has proven to be a powerful tool for studies of protein dynamics.[31–35] For instance, Reiser et al. monitored antibody protein dynamics at sub-μs temporal resolution on molecular length scales using megahertz XPCS measurements at the European X-ray free-electron laser (XFEL).[32] Typically, NPs can be used as tracers in XPCS studies or be the subject under study itself.[36–40] In contrast to FCS studies, fluorescence properties are not required in XPCS experiments and via their surface chemistry the interactions of NPs with their environment can be tuned to achieve, for instance, minimized protein adsorption or specific targeting.[6,41–45] In XPCS experiments, the sample dynamics are measured over a range of scattering vectors q, corresponding to a range of length scales, and also a very broad window of experimental characteristic times can be covered.[30,46] As an X-ray technique, it allows for probing sample dynamics in native environments without modifications of sample properties. Because gold nanoparticle (AuNP) are strong scatterers due to their electron density, they are excellent tracer particles for X-ray-based experiments in general. In XPCS experiments, their strong scattering intensity enables to measure dynamics of comparably low concentrations with high temporal resolution. In contrast to dynamic light scattering (DLS), XPCS is not affected by multiple scattering and thus allows probing the single-particle dynamics. Addressing the dynamics of NPs in biological fluids, Unni et al. investigated the rotational and translational diffusion of poly(ethylene glycol) (PEG)-coated cobalt ferrite NPs in synovial fluid and hyaluronic acid.[47] An XPCS study of the agglomeration behavior of AuNPs and their colloidal dynamics in human whole blood was presented recently.[48] An experimental challenge in such studies can be the colloidal stability of the NPs. Protein abundances have a crucial influence in this context.[49,50] NPs exposed to low protein concentrations can already aggregate, for instance, driven by unfolding of adsorbed proteins.[51] Even when the NPs are stable at moderate protein concentrations, the situation can completely change in dense protein solutions.[52,53] Agglomeration or aggregation of the NPs can then impede a meaningful analysis of colloidal structure and dynamics. In this study, we therefore probed AuNPs with a tailored PEG coating with high grafting density, that is known to exhibit excellent colloidal and chemical stability as well as minimum protein adsorption.[54–57] The structure and dynamics of these AuNP@PEG were measured in a range of bovine serum albumin (BSA) concentrations up to 4000 μM (~265 mg/mL). Albumin is the most abundant serum protein and therefore well suited to mimic physiological conditions, which we confirm by comparing to measurements in human serum. It is also commonly used as a model for macromolecular crowding.[27,58,59] We observed an excellent stability of AuNP@PEG with different PEG-shell thickness up to BSA concentrations of ~100 mg/mL. At higher concentrations, entering the range of intracellular levels and thus the regime of macromolecular crowding, the stability depends on the PEG-shell thickness. The particle dynamics stay diffusive, but significantly deviate from expectations based on

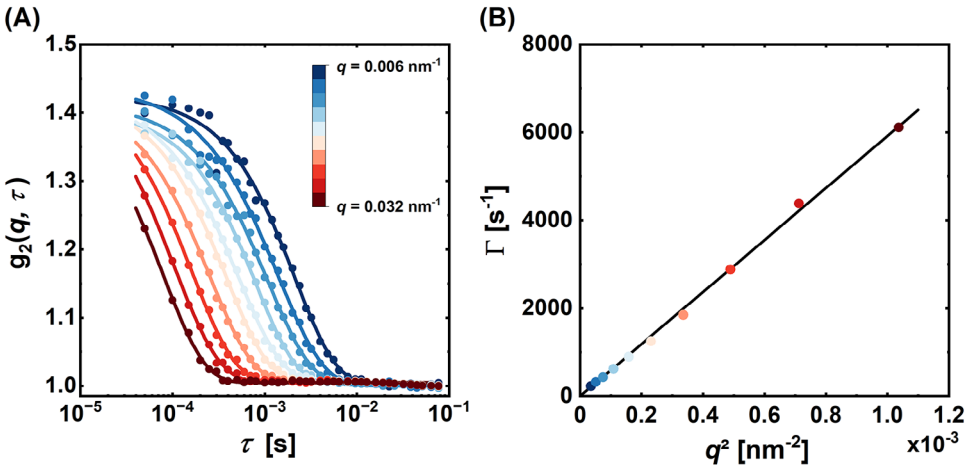

FIGURE 2 X-ray photon correlation spectroscopy (XPCS) measurements of aqueous gold nanoparticles (AuNPs). (A) Averaged autocorrelation functions of 10 individual XPCS runs as a function of the lag time τ for 10 binned q-values ranging from 0.006 to 0.032 nm^{-1}. (B) Relaxation rates Γ of the averaged autocorrelation functions as a function of squared momentum transfer q^2. Displayed solid lines represent fits to the data.

established viscosity models. The particle diffusion is faster than expected, which cannot be explained with structural changes (such as a collapse of the PEG shells). Our observations therefore point at a NP-specific contribution to the viscous properties of the dense protein solutions, namely a significantly decreased nanoscopic viscosity experienced by the PEG-coated NPs. These findings are in particular relevant in the context of nanomedicine, where polymer-coated NPs are commonly employed. Understanding that and how local properties can be affected by such nanomaterials is not only crucial to avoid misinterpretations in studies of dynamics in complex environments but also in analyzing and predicting biodistribution, pharmacokinetic properties, clearance, and local doses.

2 | RESULTS AND DISCUSSION

2.1 | Preparation, characterization, and XPCS measurements of PEG-coated AuNP

The physicochemical properties of NPs in physiological environments can be strongly affected by protein adsorption, resulting in altered pharmacokinetic properties.[6,45,60–62] PEG-based coatings, among others, have been demonstrated to minimize unwanted protein adsorption and are therefore often referred to as "stealth" or antifouling coatings for NPs.[42,44] In this study, AuNPs (core diameter $d_c \approx 50$ nm) were conjugated with α-methoxypoly(ethylene glycol)-ω-(11-mercaptoundecanoate) (PEGMUA), a PEG ligand with a hydrophobic 11-mercaptoundecanoic acid (MUA)-based spacer. This spacer enables a high grafting density of PEG polymers on the NPs and provides very high colloidal and chemical stabilization as well as minimized protein adsorption.[54,55,57] PEGMUA with molecular weights (M_w) ~2 kDa (PEGMUA2k) and ~5 kDa (PEGMUA5k) were used, corresponding to shell thicknesses of ~8 and ~12 nm and grafting densities of ~3 and ~1.7 nm^{-2}, respectively.[56] At such high grafting densities, >1 nm^{-2}, the conformation of the ligand layer is usually described as a dense brush that is considered ideal in terms of minimized protein adsorption.[63] The ζ-potential of these methoxy-terminated PEG coatings with no formal charge is slightly negative (−11.7 ± 0.6 mV).[57] The characterization of the PEGMUA-coated AuNP by transmission electron microscopy, ultraviolet/visible spectroscopy and DLS is summarized in Figure S1.

Exemplary autocorrelation functions in the q-range of 0.006 and 0.032 nm^{-1} as obtained by XPCS are shown in Figure 2A for AuNPs coated with PEGMUA5k (AuNP@PEGMUA5k) in water. To provide statistical significance and to detect potential outlier measurements, each displayed g_2-function is the result of 10 individual XPCS measurements on different positions of the same sample. An example for this procedure is provided as Figure S3. By applying an exponential fit to the autocorrelation functions (Methods, Equation 6) and fitting the so-obtained relaxation rates Γ, a diffusion coefficient $D_0 = 5.92 \times 10^{-12}$ m/s is determined. Here, the linear dependence $\Gamma \propto q^2$ is characteristic for free diffusion. Comparing XPCS and DLS results, the hydrodynamic diameters d_H obtained with the Stokes–Einstein equation (Equation 7) are in good agreement ($d_{H,XPCS} = 72.8 \pm 1.7$ nm; $d_{H,DLS} = 68.1 \pm 2.3$ nm). The hydrodynamic diameters of the other samples were in a similar range as presented in Supporting Note S2 and Table S1. The initial discussion focuses on AuNPs conjugated with the longer ligand PEGMUA5k, unless specified otherwise. In all measurements, it was ensured that radiation damage does not affect the sample dynamics (for details, we refer to Supporting Note S5 and Figures S4–S7).

Optical methods such as DLS, FCS, and nanoparticle tracking analysis (NTA) are commonly used to study the size and diffusive properties of NPs and their interactions with proteins.[43,45,62,64]

Due to the significant scattering of proteins, DLS and NTA are restricted in terms of accessible protein concentrations. This is exemplified in Figure 3A for DLS by comparing measurements of AuNP@PEGMUA5k in water, in BSA solutions at high concentrations ($c_{protein} = 100$ mg/mL), and in bovine serum ($c_{protein} = 45$ mg/mL), where the two latter ones are impeded in accurate size determination. Scattering contributions of proteins result in a size broadening and a split of the size distributions. AuNP in BSA even present a size shift due to multiple scattering, highlighting the concentration

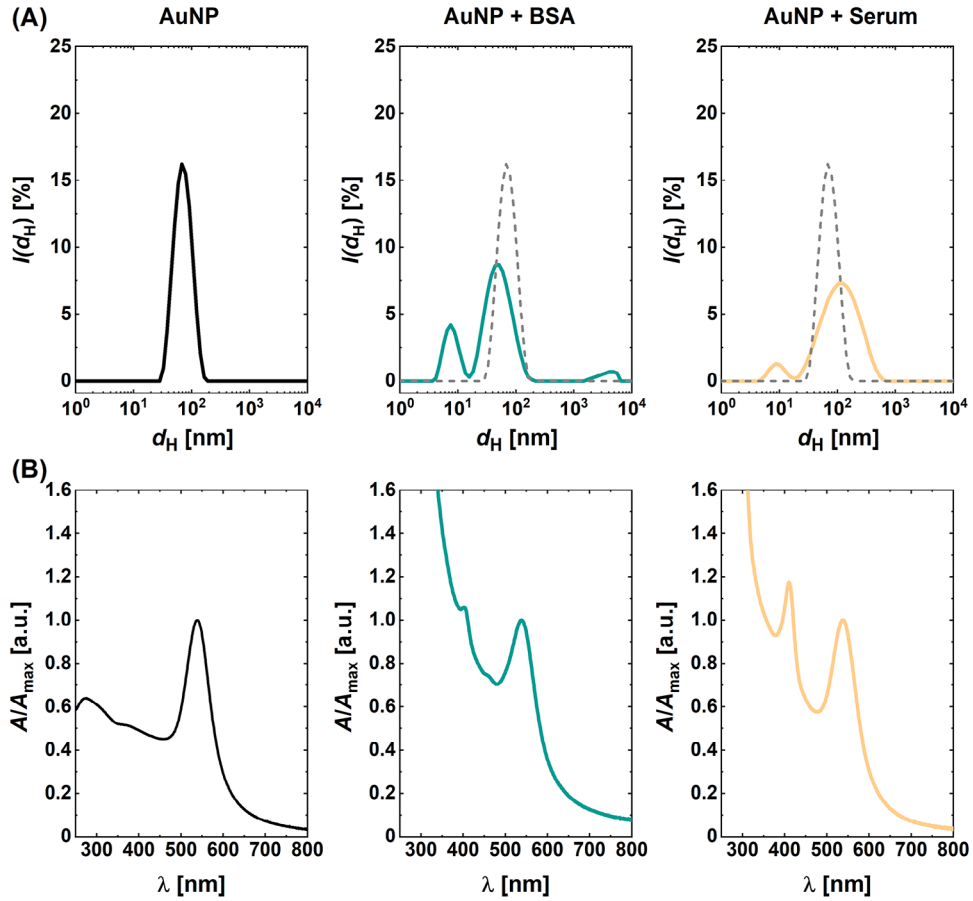

FIGURE 3 Limitations of dynamic light scattering (DLS) in dense biological fluids. (A) Intensity-weighted distributions of hydrodynamic diameters obtained by DLS: α-methoxypoly(ethylene glycol)-ω-(11-mercaptoundecanoate) (PEGMUA)-coated gold nanoparticles (AuNPs) in water, bovine serum albumin (BSA) solution ($c_{protein}$ = 100 mg/mL), and bovine serum ($c_{protein}$ = 45 mg/mL), respectively. (B) Corresponding normalized ultraviolet/visible (UV/vis) spectra. The pronounced peak in serum at λ = 410 nm corresponds to hemoglobin.

limitations of DLS.[65] Absorption spectra of the same samples (Figure 3B) underline that the AuNPs are not aggregated; aggregation would lead to a broadening and shift of the plasmon resonance band at ~535 nm due to plasmonic coupling.[61] The spectra of the protein solutions are the sum of characteristic AuNP and protein contributions to the absorbance without any indications of agglomeration or aggregation. The DLS measurements of AuNPs in protein solutions, however, do not provide reliable hydrodynamic diameters, because of the background noise caused by the large amounts of scattering proteins and thus multiple scattering processes. FCS and fluorescence cross-correlation spectroscopy circumvent some of these issues by utilizing fluorescence instead of light scattering. These methods have been used to study intracellular dynamics and protein–NP interactions.[20,28,61,66]

2.2 | The role of viscosity in analyzing dynamics

The dynamics of AuNP@PEGMUA conjugates were measured with XPCS in solutions with different BSA and bovine serum concentrations. The NP concentrations were kept constant in each set of experiments and the pH was buffered (phosphate buffered saline, PBS) at 7.4. A BSA concentration range of 0–265 mg/mL was investigated in order to represent different physiologically relevant conditions (cf. Figure 1). As potential protein-induced aggregation and protein corona formation are dynamic processes, all NP samples were incubated for the same time (2 h) in the according protein solutions before XPCS measurements were recorded. Diffusivities of AuNP@PEGMUA as a function of increasing BSA concentrations are shown in Figure 4A. For BSA concentrations larger than 10 mg/mL, the diffusivities decrease because of the increasing viscosity of the solution. Various models have been developed in order to describe the viscosity in dense protein solutions.[67–71] The viscosity model by Ross and Minton was developed for concentrated protein solutions and has been confirmed experimentally.[58,70] The modeled viscosity η_{th} is described by

$$\eta_{th} = \eta_0 \exp\left(\frac{\eta_{in}\, c_{protein}}{1 - \frac{k}{v}\,\eta_{in} c_{protein}}\right) \quad (1)$$

Here, η_0 denotes the viscosity of the initial medium (PBS), η_{in} is the intrinsic viscosity of the protein ($\eta_{in,\,BSA}$ = 4.13×10^{-3} mL/mg for pH 7, value from supplier), $c_{protein}$ is the protein concentration, k is a crowding factor, and v is a shape factor for non-spherical particles. The model accounts for excluded volume effects and their influence on the solution viscosity. The accuracy of this approximation varies, depending on the specific protein and experimental conditions, for example, the pH value.[58] Yadav et al. determined a reasonable value of k/v = 0.45 for BSA[58] based on prior

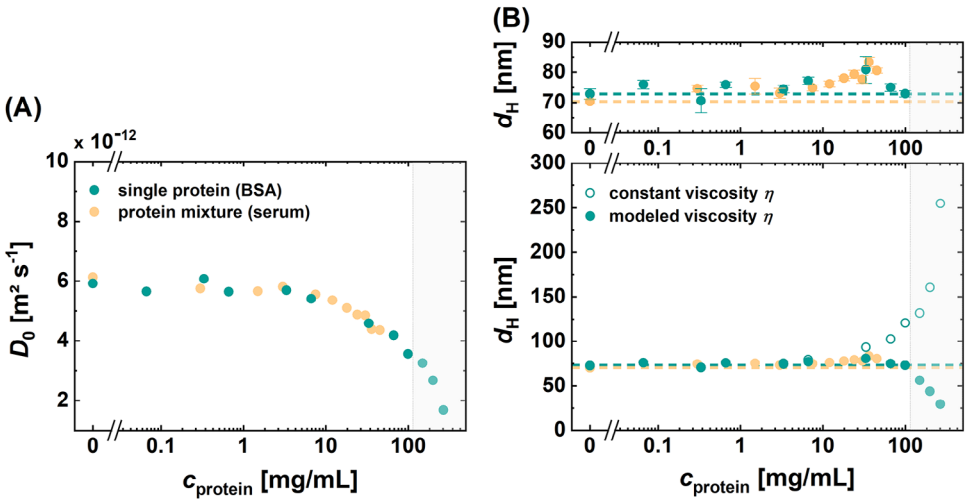

FIGURE 4 Evolution of nanoparticle (NP) dynamics and hydrodynamic diameter with increasing bovine serum albumin (BSA) (teal) and bovine serum (orange) concentration. (A) Diffusion coefficients of AuNP@PEGMUA5k as a function of protein concentration. (B) Calculated hydrodynamic diameters d_H as a function of protein concentration. Empty data points represent d_H values calculated with constant viscosity and filled dots with modeled viscosity obtained by the Ross and Minton equation. The protein concentration range, where the viscosity model does not agree with the data anymore is highlighted in gray. The dashed lines mark the NP sizes in aqueous condition. The top part of (B) shows a tighter *y*-axis scaling of the range of $c_{protein}$ = 0–100 mg/mL for a better visualization of the size fluctuations. AuNP, gold nanoparticles; PEGMUA, α-methoxypoly(ethylene glycol)-ω-(11-mercaptoundecanoate).

studies on hemoglobin[70] and IgG_1,[71] which was used in the following.

The effective hydrodynamic diameters d_H were calculated with the Stokes–Einstein equation (Equation 7) using the diffusion coeffcients D_0 determined from the XPCS measurements and the viscosities from the Ross–Minton model (Equation 1). In the BSA concentration range up to 100 mg/mL, we find no indications of protein-induced aggregation or agglomeration but good agreement of the hydrodynamic diameters with the corresponding values in water as shown in Figure 4B. Exact values are listed in Supporting Note S3 and Table S2. Only a slight size fluctuation ($\Delta d_{H,average} \approx 2.4$ nm) was observed. This accuracy is not sufficient to confidently rule out any BSA adsorption, for example, in sub-monolayer coverages, but we find no trends that suggest an adsorption isotherm as would be characteristic for protein adsorption.[61] Taken together, we conclude that protein-induced aggregation of NPs is unlikely to play a major role and that no indications of significant protein adsorption to the AuNP@PEGMUA were observed in the BSA concentration range up to 100 mg/mL. These findings underline the excellent stabilization and bio-repulsive properties provided by the PEGMUA coatings.

For NPs exposed to bovine serum, obtained diffusion coefficients and hydrodynamic diameters are in excellent agreement with the BSA measurements, including their dependence on protein concentration. This underlines once more the stabilization of the samples and robust surface chemistry (two different batches of AuNP@PEGMUA are compared), but also shows that the viscosity model can be generalized to some extent to more complex protein mixtures. Only when comparing the deviation of measurements in serum and in water it seems that the viscosity correction is slightly better in the BSA case compared to the measurements in serum. To illustrate the increasing effect of viscosity on size determination at high protein concentrations, Figure 4B (bottom) shows the calculated hydrodynamic diameters when assuming a constant viscosity.

We conclude that the AuNP@PEGMUA conjugates are well stabilized and that their dynamics in protein solutions up to ~100 mg/mL can be well described by free diffusion according to the Stokes–Einstein model when accounting carefully for the changing viscosity at higher protein concentrations. This protein concentration (~100 mg/mL) is well above the total protein concentration in serum, however, in the cytosol of cells protein concentrations can be significantly higher and the regime of macromolecular crowding is reached.[17,72] In the data presented in Figure 4B (bottom), it can be appreciated clearly, that in the regime of high BSA concentrations (>100 mg/mL), the calculated hydrodynamic diameters strongly deviate from the expectation, even with the viscosity correction. The sample dynamics at high BSA concentrations are therefore analyzed in more detail in the following section.

2.3 | Dynamics in the regime of macromolecular crowding

Hydrodynamic diameters differ strongly from the expected size for the three highest BSA concentrations that have been measured. The smaller d_H values suggest significant faster dynamics than expected in this crowded environment. In contrast to reports on intracellular dynamics of proteins and particles with superdiffusive behavior due to active intracellular transport,[73–76] we find no indications of anomalous dynamics. All investigated AuNP@PEGMUA samples in BSA and bovine serum undergo free diffusion even at the highest BSA concentration. This is expectable, as for active intracellular transport motor proteins and corresponding "tracks", such as the kinesin–microtubule system are needed. A comprehensive analysis of the diffusive behavior can be found in Supporting Note S7. A more likely explanation lies in the applied viscosity model by Ross and Minton. Figure 5 illustrates the deviations of viscosities experienced by the NPs from the Ross and Minton model for both

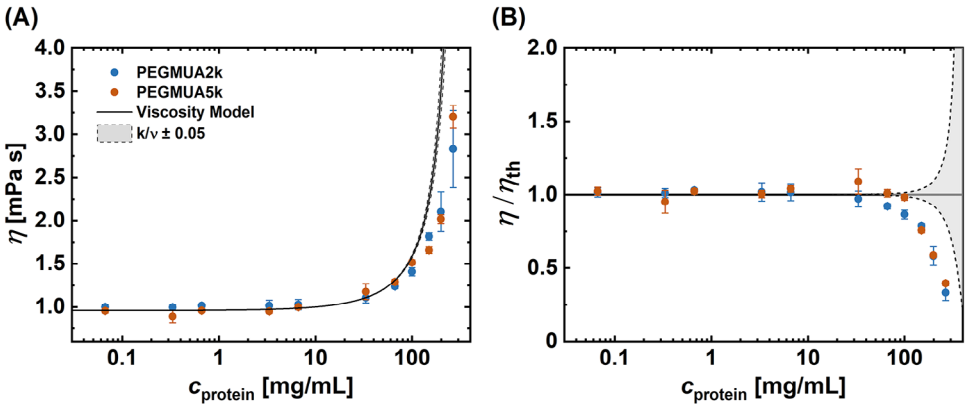

FIGURE 5 Comparison of the viscosity model by Ross and Minton with viscosities determined experimentally assuming a constant hydrodynamic diameter of the nanoparticle (NP). (A) Dependence of the viscosity η on the protein concentration for NPs coated with PEGMUA2k (blue) and PEGMUA5k (red) and the values predicted by the applied viscosity model (black line). The effect of varying k/v by ±0.05 is indicated by the gray shading. (B) Same data but with the relative viscosity η/η_{th}. PEGMUA, α-methoxypoly(ethylene glycol)-ω-(11-mercaptoundecanoate).

PEGMUA2k and PEGMUA5k. Nanoscale viscosities η were calculated by assuming a constant particle size d_H and using the diffusion coefficient D_0 as determined from the XPCS measurements. For concentrations exceeding 100 mg/mL, nanoscopic viscosities are notably lower as predicted, even though the model is generally suitable for protein densities in that range and was experimentally confirmed.[58,67,70,71] As a semi-empirical model, the viscosity determination relies on the experimentally determined crowding and shape factor k/v. To investigate the potential influence of k/v on the theoretical predictions, its value was varied by ±0.05. The impact of k/v on the model accuracy is presented in Figure 5B by the gray shading. To illustrate the margin due to the variation of k/v more clearly, normalized viscosity values η/η_{th} are used. Despite the wide range covered by the variation of k/v and its increasing relevance at high BSA concentrations, the faster NP dynamics still do not align with the model's predictions. In complementary microrheology experiments, we tested the macroscopic viscosity of BSA solutions with and without AuNP@PEGMUA. The results were in agreement with the model and notably we observed no significant difference of the viscosities in the presence of AuNP@PEGMUA in these experiments (Supporting Note S6 and Figure S8).

As discussed by Yadav et al., when analyzing the viscosity behavior of BSA solutions at high concentrations, intermolecular forces cannot be neglected.[58] Hence, one explanation for the reduced nanoscopic viscosity might be the repulsive properties of the NP's PEG coating leading to a disruption of transient networks formed by the BSA molecules. These transient networks increase the diffusive resistance and accordingly the local viscosity decreases when they are disrupted.[23,77] Unni et al. observed a similar discrepancy in the viscosity of NPs dispersed in synovial fluid and hyaluronic acid.[47] In their study, macroscopic shear viscosity of synovial fluid determined by rheology strongly deviated from the nanoscopic viscosity experienced by PEG-coated cobalt ferrite NPs. Thus, we can confirm their important findings for the most abundant serum protein BSA, where the effect is much weaker compared to hyaluronic acid—the major component of synovial fluid that determines its viscous properties—but still significant. For the strongly network-forming glycosaminoglycan hyaluronic acid, the nanoscale viscosities in the presence of PEG-coated NPs were several orders of magnitude smaller than expected for solutions above 1 mg/mL. For the BSA solutions at high concentrations (>100 mg/mL) studied herein, we find a factor in the range 1–3. Even though this effect is much more subtle, it is still significant and has to be considered in analyses of intracellular dynamics and transport of NPs.

In the final section, the role of PEG-coating thickness in terms of colloidal stability will be discussed.

2.4 | The role of PEGMUA-coating thickness

The influence of PEG-coating thickness on the colloidal stability was investigated by comparing the dynamics of AuNPs coated with different PEGMUA ligand lengths. PEGMUA2k ($M_w \sim 2000$ g/mol) and PEGMUA5k ($M_w \sim 5000$ g/mol) coatings were studied, corresponding to shell thicknesses s in the range 6–9 nm (2k) and 12–14 nm (5k) according to previous studies.[54–56] AuNP@PEGMUA2k exhibited some indications of structural changes at high protein concentrations, whereas AuNP@PEGMUA5k seemed to be colloidally stable in the whole measured BSA concentration range. Figure 6 summarizes the measurements, with the q-dependence of τ representing the dynamics and the $I(q)$ representing the structure of the samples. For AuNP@PEGMUA2k at high BSA concentrations, the upturn of the $I(q)$ at low q (Figure 6D) and the non-linear q-dependence of τ (Figure 6C) indicate structural changes of the samples, such as agglomeration or aggregation, leading to changed dynamics. A closer look at the q-dependency of the relaxation times τ for the investigated q-range reveals length-scale dependent behavior deviating from homogeneous dynamics in the system (Figures 6C, S9, and S10). The calculated hydrodynamic diameters for AuNP@PEGMUA2k in comparison to AuNP@PEGMUA5k are shown in Figure S2. In contrast, NPs that are conjugated with PEGMUA5k exhibit a consistent and homogeneous diffusion behavior, indicating excellent colloidal stability across the entire range of protein concentrations studied. This underlines the importance of thorough experimental testing of colloidal stability in this context. Even when the colloidal stability is immaculate at comparably high protein concentrations up to 100 mg/mL, it might still be reduced at protein concentrations which are

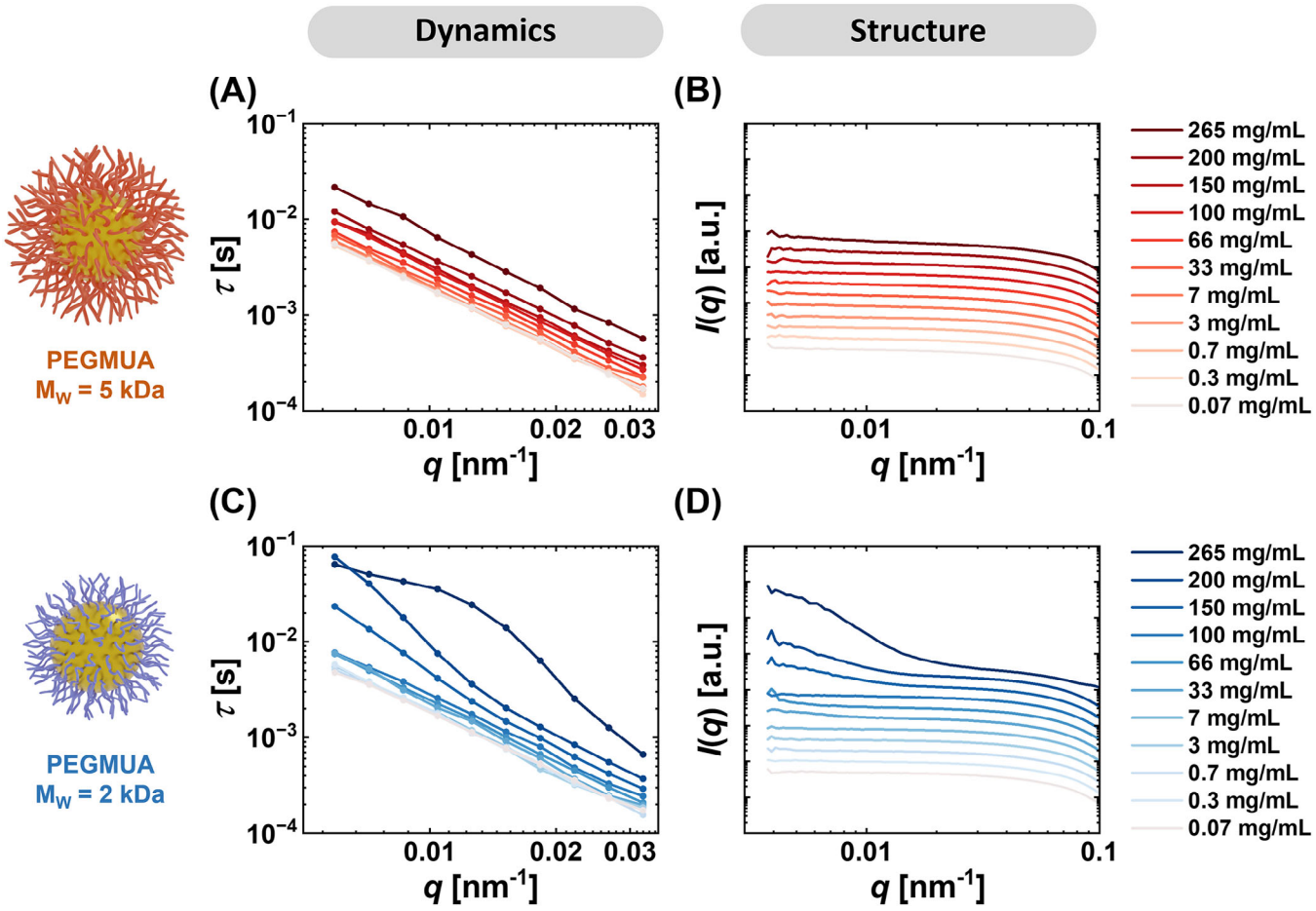

FIGURE 6 Colloidal stability of nanoparticles (NPs) with different α-methoxypoly(ethylene glycol)-ω-(11-mercaptoundecanoate) (PEGMUA) ligand lengths for varying bovine serum albumin (BSA) concentrations. q-dependency of the relaxation time τ and small-angle X-ray scattering (SAXS) scattering intensity as a function of the scattering vector q of NPs coated with PEGMUA5k (A and B) and PEGMUA2k (C and D) for a BSA concentration range of 0.07–265 mg/mL.

even higher (>100 mg/mL), but nonetheless physiologically very relevant, because they represent intracellular levels.

3 | CONCLUSIONS

In conclusion, we find an excellent colloidal stability for AuNP@PEGMUA5k in physiologically relevant high protein concentrations representing intracellular levels. AuNP@PEGMUA2k also exhibit good colloidal stability, which is, however, slightly impaired at BSA concentrations >100 mg/mL. Studying the colloidal dynamics of AuNP@PEGMUA5k over a large range of BSA concentrations with XPCS, we find viscosities at high BSA concentrations that significantly differ from expectations based on well-established models and complementary rheology experiments. This might be explained with the bio-repulsive properties of the PEG coatings leading to a nanoscopic viscosity that differs from the macroscopic viscosity of BSA solutions. Our findings are relevant for nanomedicine and NP-based in vitro studies, where PEG coatings, and other polymer coatings in general, are commonly employed. Biological systems are very complex, not only in terms of structure but also in terms of dynamics, and a thorough understanding of the diffusive properties of nanomaterials is crucial for their safe and successful application. XPCS studies can make valuable contributions in this respect, because they allow to correlate structure and dynamics over large and relevant spatial and temporal ranges.

4 | EXPERIMENTAL

4.1 | Materials

BSA (≥96%), tetrachloroauric(III) acid trihydrate (≥99.9% trace metal basis) and sodium citrate dihydrate (>99.0%) were purchased from Sigma Aldrich. PBS (w/o Mg, Ca) was purchased from Cytiva. Bovine serum (lyophilized powder) was purchased from United States Biological. For bovine serum, the total protein concentration was determined by the commercial supplier by a Bradford assay with an IgG standard curve to be 60 mg/mL. PEGMUA (2 and 5 kDa) was synthesized and characterized as described previously.[54]

4.2 | Synthesis and characterization of AuNPs

AuNPs were synthesized according to a seeded-growth method presented by Bastús et al.[78] Details of the synthesis, functionalization and characterization are provided as Supporting Note S1.

4.3 | Sample preparation

In situ coherent X-ray scattering measurements were performed in quartz capillaries ($\emptyset$ = 1 mm, wall thickness = 0.01 mm). BSA stock solutions were prepared using PBS. To assure equivalent conditions, NP concentrations were kept constant (c_{NP} = 10 nM) and NPs exposed to BSA and bovine serum were incubated for 2 h before the respective measurements. Control experiments with identical measurement conditions were carried out for each investigated BSA and bovine serum concentrations without the addition of NPs.

4.4 | Scattering experiments at ID02 beamline

XPCS experiments were performed at ID02 at the European Synchrotron Radiation Facility, Grenoble, France. An ultra-small-angle X-ray scattering geometry was used with a sample-to-detector distance of 30.7 m allowing access to a q-range of 0.0038–0.11 nm^{-1}. The X-ray photon energy was set to 12.2 keV. The partially coherent X-ray beam was focused by compound refractive lenses to a beam size of 40 × 25 μm^2. Two-dimensional scattering patterns were recorded with an Eiger2×4M (pixel size 75 × 75 μm^2) and speckle patterns were obtained with an Eiger500k detector (pixel size 75 × 75 μm^2) at a maximum framing rate of 23 kHz. Preliminary exposures were performed to determine the ideal measurement conditions. Measurements followed a strict procedure to exclude radiation-induced alteration of the sample. Initially, five single shot exposures with varying durations (0.002, 0.01, 0.05, 0.1, and 0.25 s) were carried out, followed by 10 individual series of 2000 diffraction patterns with a single exposure time of 0.02 ms and a detector deadtime of 0.03 ms after exposures. In between measurements, the sample was spatially displaced to prevent repeated exposures at the same capillary position. Each sample was investigated at different photon flux by implementing Zr- or Mo-based beam attenuators.

4.5 | X-ray photon correlation spectroscopy analysis

In XPCS experiments, the dynamics of the sample are obtained via the intensity–intensity correlation function

$$g_2(q,\ \tau) = \frac{\langle I(q,t) \cdot I(q,t+\tau)\rangle}{\langle I(q,t)\rangle^2}, \tag{2}$$

with the intensity $I(q,t)$ measured typically by a 2D detector at time t and wave vector transfer q. The average is taken for pixels within the same q bin of modulus

$$q = \frac{4\pi}{\lambda} \sin\frac{2\theta}{2}, \tag{3}$$

where 2θ denotes the scattering angle and λ denotes the wavelength. Via the Siegert relation, the correlation function g_2 is connected to the intermediate scattering function $g_1(q,\tau)$ via

$$g_2(q,\ \tau) = 1 + \beta(q)|g_1(q,\ \tau)|^2. \tag{4}$$

Here, β is the so-called speckle contrast that depends on the coherence properties of the radiation and the experimental geometry. For many systems, it is expressed by a Kohlrausch–Williams–Watts (KWW) function as

$$g_1(q,\ \tau) = \exp\left[-(\Gamma(q)\cdot\tau)^{\gamma}\right] \tag{5}$$

and thus

$$g_2(q,\ \tau) = 1 + \beta\exp\left[-2(\Gamma\cdot\tau)^{\gamma}\right]. \tag{6}$$

The KWW exponent γ is a measure of the distribution of relaxation times in the studied sample volume. Diffusion processes are characterized by $\gamma = 1$. Furthermore, the relaxation rate Γ or the relaxation time $\tau_0 = 1/\Gamma$ shows a particular q-dependence that is usually given by a power law $\Gamma \propto q^p$. A square dependence ($p = 2$) is found for diffusive dynamics, while sub- and super-diffusion are expressed by $p > 2$ and $p < 2$, respectively. In case of free self-diffusion, XPCS allows measuring the Stokes–Einstein diffusion constant

$$D_0 = \frac{k_B T}{3\pi\eta d_H} \tag{7}$$

directly via $\Gamma = D_0 q^2$. Moreover, as a real-time probe the access to heterogeneous dynamics is possible by XPCS. Further information is given in Supporting Notes S4 and S5.

ACKNOWLEDGMENTS

F.O. and W.J.P. acknowledge funding by the Deutsche Forschungsgemeinschaft (DFG, GRK 2536). We acknowledge European Synchrotron Radiation Facility (ESRF) (Grenoble, France) for the provision of experimental facilities. We are grateful to Thomas Zinn and Theyencheri Narayanan for their provided assistance and fruitful discussions at the beamline ID02 at the ESRF. The beamtime was allocated for proposal SC 5173. F.L. acknowledges support from the Cluster of Excellence: Advanced Imaging of Matter of the DFG (EXC 2056, Project 390715994). The authors also acknowledge the scientific exchange and support of the Centre for Molecular Water Science.

CONFLICT OF INTEREST STATEMENT

The authors declare they have no conflicts of interest.

ORCID

Florian Schulz https://orcid.org/0000-0003-4440-3680

REFERENCES

1. S. M. Moghimi, A. C. Hunter, J. C. Murray, *FASEB J.* **2005**, *19*, 311.
2. E. Boisselier, D. Astruc, *Chem. Soc. Rev.* **2009**, *38*, 1759.
3. B. Y. S. Kim, J. T. Rutka, W. C. W. Chan, *N. Engl. J. Med.* **2010**, *363*, 2434.
4. E. C. Dreaden, A. M. Alkilany, X. Huang, C. J. Murphy, M. A. El-Sayed, *Chem. Soc. Rev.* **2012**, *41*, 2740.
5. X. Yang, M. Yang, B. Pang, M. Vara, Y. Xia, *Chem. Rev.* **2015**, *115*, 10410.

6. P. Chun Ke, S. Lin, W. J. Parak, T. P. Davis, F. Caruso, *ACS Nano* **2017**, *11*, 11773.
7. B. Pelaz, C. Alexiou, R. A. A. Puebla, F. Alves, A. M. Andrews, S. Ashraf, L. P. Balogh, L. Ballerini, A. Bestetti, C. Brendel, S. Bosi, M. Carril, W. C. W. Chan, C. Chen, X. Chen, X. Chen, Z. Cheng, D. Cui, J. Du, C. Dullin, A. Escudero, N. Feliu, M. Gao, M. George, Y. Gogotsi, A. Grünweller, Z. Gu, N. Halas, N. Hampp, R. K. Hartmann, M. C. Hersam, P. Hunziker, J. Jian, X. Jiang, P. Jungebluth, P. Kadhiresan, K. Kataoka, A. Khademhosseini, J. Kopecek, N. A. Kotov, H. F. Krug, D. S. Lee, C.-M. Lehr, K. W. Leong, X.-J. Liang, M. L. Lim, L. M. L. Marzán, X. Ma, P. Macchiarini, H. Meng, H. Möhwald, P. Mulvaney, A. E. Nel, S. Nie, P. Nordlander, T. Okano, J. Oliveira, T. H. Park, R. M. Penner, M. Prato, V. Puntes, V. M. Rotello, A. Samarakoon, R. E. Schaak, Y. Shen, S. Sjöqvist, A. G. Skirtach, M. G. Soliman, M. M. Stevens, H.-W. Sung, B. Z. Tang, R. Tietze, B. N. Udugama, J. S. VanEpps, T. Weil, P. S. Weiss, I. Willner, Y. Wu, L. Yang, Z. Yue, Q. Zhang, Q. Zhang, X. E. Zhang, Y. Zhao, X. Zhou, W. J. Parak, *ACS Nano* **2017**, *11*, 2313.
8. K. Luby-Phelps, *Int. Rev. Cytol.* **1999**, *192*, 189.
9. H.-X. Zhou, G. Rivas, A. P. Minton, *Annu. Rev. Biophys.* **2008**, *37*, 375.
10. H. X. Zhou, *Arch. Biochem. Biophys*. **2008**, *469*, 76.
11. S. B. Zimmerman, S. O. Trach, *J. Mol. Biol.* **1991**, *222*, 599.
12. A. B. Fulton, *Cell* **1982**, *30*, 345.
13. S. Cayley, B. A. Lewis, H. J. Guttman, M. T. Record, *J. Mol. Biol.* **1991**, *222*, 281.
14. R. J. Ellis, *Curr. Opin. Struct. Biol.* **2001**, *11*, 114.
15. R. J. Ellis, *Trends Biochem. Sci.* **2001**, *26*, 597.
16. R. J. Ellis, A. P. Minton, *Nature* **2003**, *425*, 27.
17. G. Rivas, A. P. Minton, *Trends Biochem. Sci.* **2016**, *41*, 970.
18. A. H. Elcock, *Curr. Opin. Struct. Biol.* **2010**, *20*, 196.
19. H. Neuweiler, M. Löllmann, S. Doose, M. Sauer, *J. Mol. Biol.* **2007**, *365*, 856.
20. S. A. Kim, K. G. Heinze, P. Schwille, *Nat. Methods* **2007**, *4*, 963.
21. S. Zorrilla, M. A. Hink, A. J. W. G. Visser, M. P. Lillo, *Biophys. Chem.* **2007**, *125*, 298.
22. Y. Wang, C. Li, G. J. Pielak, *J. Am. Chem. Soc.* **2010**, *132*, 9392.
23. Q. Wang, A. Zhuravleva, L. M. Gierasch, *Biochemistry* **2011**, *50*, 9225.
24. C. Zhang, Z. Jin, B. Zeng, W. Wang, G. Palui, H. Mattoussi, *J. Phys. Chem. B* **2020**, *124*, 4631.
25. M. Carril, D. Padro, P. del Pino, C. Carrillo-Carrion, M. Gallego, W. J. Parak, *Nat. Commun.* **2017**, *8*, 1542.
26. D. Padro, P. Cienskowski, S. Lopez-Fernandez, I. Chakraborty, C. Carrillo-Carrion, N. Feliu, W. J. Parak, M. Carril, *Small* **2020**, *16*, 2001160.
27. S. Bucciarelli, J. S. Myung, B. Farago, S. Das, G. A. Vliegenthart, O. Holderer, R. G. Winkler, P. Schurtenberger, G. Gompper, A. Stradner, *Sci. Adv.* **2016**, *2*, e1601432.
28. M. Wachsmuth, W. Waldeck, J. Langowski, *J. Mol. Biol.* **2000**, *298*, 677.
29. J. H. Jeon, V. Tejedor, S. Burov, E. Barkai, C. Selhuber-Unkel, K. Berg-Sorensen, L. Oddershede, R. Metzler, *Phys. Rev. Lett.* **2011**, *106*, 048103.
30. F. Lehmkühler, W. Roseker, G. Grübel, *Appl. Sci.* **2021**, 11, 6179.
31. A. Girelli, H. Rahmann, N. Begam, A. Ragulskaya, M. Reiser, S. Chandran, F. Westermeier, M. Sprung, F. Zhang, C. Gutt, F. Schreiber, *Phys. Rev. Lett.* **2021**, *126*, 138004.
32. M. Reiser, A. Girelli, A. Ragulskaya, S. Das, S. Berkowicz, M. Bin, M. Ladd-Parada, M. Filianina, H.-F. Poggemann, N. Begam, M. Sayed Akhundzadeh, S. Timmermann, L. Randolph, Y. Chushkin, T. Seydel, U. Boesenberg, J. Hallmann, J. Möller, A. Rodriguez-Fernandez, R. Rosca, R. Schaffer, M. Scholz, R. Shayduk, A. Zozulya, A. Madsen, F. Schreiber, F. Zhang, F. Perakis, C. Gutt, *Nat. Commun.* **2022**, 13.
33. J. Möller, M. Sprung, A. Madsen, C. Gutt, *IUCrJ* **2019**, *6*, 794.
34. F. Perakis, C. Gutt, *Phys. Chem. Chem. Phys.* **2020**, *22*, 19443.
35. M. Bin, M. Reiser, M. Filianina, S. Berkowicz, S. Das, S. Timmermann, W. Roseker, R. Bauer, J. Öström, A. Karina, K. Amann-Winkel, M. Ladd-Parada, F. Westermeier, M. Sprung, J. Möller, F. Lehmkühler, C. Gutt, F. Perakis, *J. Phys. Chem. B* **2023**, *127*, 4922.
36. C. Caronna, Y. Chushkin, A. Madsen, A. Cupane, *Phys. Rev. Lett.* **2008**, *100*, 055702.
37. H. Conrad, F. Lehmkühler, B. Fischer, F. Westermeier, M. A. Schroer, Y. Chushkin, C. Gutt, M. Sprung, G. Grübel, *Phys. Rev. E* **2015**, *91*, 042309.
38. H. Guo, G. Bourret, M. K. Corbierre, S. Rucareanu, R. B. Lennox, K. Laaziri, L. Piche, M. Sutton, J. L. Harden, R. L. Leheny, *Phys. Rev. Lett.* **2009**, *102*, 075702.
39. B. Ruta, O. Czakkel, Y. Chushkin, F. Pignon, R. Nervo, F. Zontone, M. Rinaudo, *Soft Matter* **2014**, *10*, 4547.
40. T. Koga, N. Jiang, P. Gin, M. K. Endoh, S. Narayanan, L. B. Lurio, S. K. Sinha, *Phys. Rev. Lett.* **2011**, *107*, 225901.
41. N. Feliu, D. Docter, M. Heine, P. Del Pino, S. Ashraf, J. Kolosnjaj-Tabi, P. Macchiarini, P. Nielsen, D. Alloyeau, F. Gazeau, R. H. Stauber, W. J. Parak, *In Vivo Degeneration and the Fate of Inorganic Nanoparticles*, *Vol. 45*, Royal Society of Chemistry **2016**, 2440.
42. J. V. Jokerst, T. Lobovkina, R. N. Zare, S. S. Gambhir, *Nanomedicine* **2011**, *6*, 715.
43. M. S. Bannon, A. López Ruiz, K. Corrotea Reyes, M. Marquez, Z. Wallizadeh, M. Savarmand, C. A. LaPres, J. Lahann, K. McEnnis, *Part. Part. Syst. Charact.* **2021**, 38.
44. P. Bevilacqua, S. Nuzzo, E. Torino, G. Condorelli, M. Salvatore, A. M. Grimaldi, *Nanomaterials* **2021**, *11*, 780.
45. W. Wu, Q. Wu, Q. Liu, Y. Li, P. Ren, Y. Wu, F. Chen, *Chin. J. Anal. Chem.* **2023**, 51.
46. A. Jain, F. Schulz, F. Dallari, V. Markmann, F. Westermeier, Y. G. Zhang, G. Grubel, F. Lehmkuhler, *J. Chem. Phys.* **2022**, *157*, 184901.
47. M. Unni, S. Savliwala, B. D. Partain, L. Maldonado-Camargo, Q. Zhang, S. Narayanan, E. M. Dufresne, J. Ilavsky, P. Grybos, A. Koziol, P. Maj, R. Szczygiel, K. D. Allen, C. M. Rinaldi-Ramos, *Sci. Adv.* **2021**, 7.
48. F. Otto, X. Sun, F. Schulz, C. Sanchez-Cano, N. Feliu, F. Westermeier, W. J. Parak, *Small* **2022**, *18*, 2201324.
49. J. Piella, N. G. Bastús, V. Puntes, *Bioconjugate Chem.* **2017**, *28*, 88.
50. A. Tukova, Y. Nie, M. Tavakkoli Yaraki, N. T. Tran, J. Wang, A. Rodger, Y. Gu, Y. Wang, *Aggregate* **2023**, *4*, e323.
51. S. Dominguez-Medina, L. Kisley, L. J. Tauzin, A. Hoggard, B. Shuang, A. S. D. S. Indrasekara, S. Chen, L.-Y. Wang, P. J. Derry, A. Liopo, E. R. Zubarev, C. F. Landes, S. Link, *ACS Nano* **2016**, *10*, 2103.
52. S. J. Soenen, W. J. Parak, J. Rejman, B. Manshian, *Chem. Rev.* **2015**, *115*, 2109.
53. D. Valdeperez, N. Wutke, L.-M. Ackermann, W. J. Parak, M. Klapper, B. Pelaz, *Inorg. Chim. Acta* **2022**, *534*, 120820.
54. F. Schulz, T. Vossmeyer, N. G. Bastus, H. Weller, *Langmuir* **2013**, *29*, 9897.
55. F. Schulz, G. T. Dahl, S. Besztejan, M. A. Schroer, F. Lehmkühler, G. Grübel, T. Vossmeyer, H. Lange, *Langmuir* **2016**, *32*, 7897.
56. F. Schulz, J. Möller, F. Lehmkühler, A. J. Smith, T. Vossmeyer, H. Lange, G. Grübel, M. A. Schroer, *Part. Part. Syst. Charact.* **2018**, *35*, 1700319.
57. F. Hoeg, J. Schulz, S. Graf, D. Salah, S. Chandralingam, W. Maison, W. J. Parak, F. Schulz, *J. Phys. Chem. C* **2022**, *126*, 20594.
58. S. Yadav, S. J. Shire, D. S. Kalonia, *Pharm. Res.* **2011**, *28*, 1973.
59. F. Roosen-Runge, M. Hennig, F. Zhang, R. M. J. Jacobs, M. Sztucki, H. Schober, T. Seydel, F. Schreiber, *Proc. Natl. Acad. Sci. U. S. A.* **2011**, *108*, 11815.
60. H. Wang, Y. Lin, K. Nienhaus, G. U. Nienhaus, *Wiley Interdiscip. Rev. Nanomed. Nanobiotechnol.* **2018**, 10, e1500.
61. C. Röcker, M. Pötzl, F. Zhang, W. J. Parak, G. U. Nienhaus, *Nat. Nanotechnol.* **2009**, *4*, 577.
62. C. Carrillo-Carrion, M. Carril, W. J. Parak, *Techniques for the Experimental Investigation of the Protein Corona*, *Vol. 46*, Elsevier Ltd. **2017**, 106.
63. Q. Yang, S. W. Jones, C. L. Parker, W. C. Zamboni, J. E. Bear, S. K. Lai, *Mol. Pharmaceutics* **2014**, *11*, 1250.
64. J. Toro-Mendoza, L. Maio, M. Gallego, F. Otto, F. Schulz, W. J. Parak, C. Sanchez-Cano, I. Coluzza, *ACS Nano* **2023**, *17*, 955.
65. T. Zheng, S. Bott, Q. Huo, *ACS Appl. Mater. Interfaces* **2016**, *8*, 21585.
66. J. T. Mika, B. Poolman, *Curr. Opin. Biotechnol.* **2011**, *22*, 117.
67. W. J. Galush, L. N. Le, J. M. R. Moore, *J. Pharm. Sci.* **2012**, *101*, 1012.
68. A. D. Gonçalves, C. Alexander, C. J. Roberts, S. G. Spain, S. Uddin, S. Allen, *RSC Adv.* **2016**, *6*, 15143.
69. I. M. Krieger, T. J. Dougherty, *Trans. Soc. Rheol.* **1959**, *3*, 137.
70. P. D. Ross, A. P. Minton, *Biochem. Biophys. Res. Commun.* **1977**, *76*, 971.

71. S. Yadav, S. J. Shire, D. S. Kalonia, *J. Pharm. Sci.* **2010**, *99*, 4812.
72. S. B. Zimmerman, A. P. Minton, *Annu. Rev. Biophys. Biomol. Struct.* **1993**, *22*, 27.
73. A. Caspi, R. Granek, M. Elbaum, *Phys. Rev. Lett.* **2000**, *85*, 5655.
74. N. Gal, D. Weihs, *Phys. Rev. E* **2010**, *81*, 020903.
75. J. F. Reverey, J.-H. Jeon, H. Bao, M. Leippe, R. Metzler, C. Selhuber-Unkel, *Sci. Rep.* **2015**, *5*, 11690.
76. K. Chen, B. Wang, S. Granick, *Nat. Mater.* **2015**, *14*, 589.
77. J. R. Perkins, I. Diboun, B. H. Dessailly, J. G. Lees, C. Orengo, *Structure* **2010**, *18*, 1233.
78. N. G. Bastús, J. Comenge, V. Puntes, *Langmuir* **2011**, *27*, 11098.

SUPPORTING INFORMATION

Additional supporting information can be found online in the Supporting Information section at the end of this article.

How to cite this article: F. Otto, F. Dallari, F. Westermeier, D. C. F. Wieland, W. J. Parak, F. Lehmkühler, F. Schulz, *Aggregate* **2024**, *5*, e483. https://doi.org/10.1002/agt2.483